AD-A145 941 VECTOR MAGNETIC FIELD ANALYSIS OF LORENTZ FORCES ACTING IN THE SOLAR ATMOSPHERE(U) ALABAMA UNIV IN HUNTSVILLE K KRALL ET AL. 28 NOV 83 AFGL-TR-83-0314 1/1

UNCLASSIFIED F19628-82-K-0014 F/G 3/2 NL

END

FILMED

DTIC

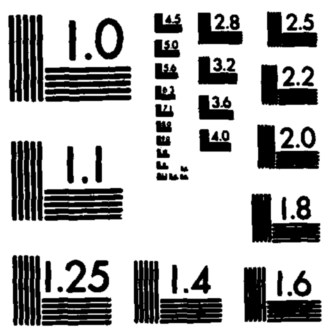


MICROCOPY RESOLUTION TEST CHART

(12)

AFGL-TR-83-0314

# VECTOR MAGNETIC FIELD ANALYIS OF LORENTZ FORCES ACTING IN THE SOLAR ATMOSPHERE


K. Krall
S. T. Wu
J. B. Smith, Jr.





The University of Alabama in Huntsville
Huntsville, AL 35899


Final Report
3 December 1981 - 31 July 1983

28 November 1983

Approved for public release; distribution unlimited



AIR FORCE GEOPHYSICS LABORATORY
AIR FORCE SYSTEMS COMMAND
UNITED STATES AIR FORCE
HANSCOM AFB, MASSACHUSETTS 01731

This report has been reviewed by the ESD Public Affairs Office (PA) and is releasable to the National Technical Information Service (NTIS).

This technical report has been reviewed and is approved for publication

Donald F. Neidig | Donald F. Neidig, Acting for
---|---
(Signature) | (Signature)
DONALD F. NEIDIG | STEPHEN L. KEIL, Capt, USAF
Contract Manager | Branch Chief

FOR THE COMMANDER

RC Sagalyn
(Signature)
R. C. SAGALYN
Division Director

Qualified requestors may obtain additional copies from the Defense Technical Information Center. All others should apply to the National Technical Information Service.

If your address has changed, or if you wish to be removed from the mailing list, or if the addressee is no longer employed by your organization, please notify AFGL/DAA, Hanscom AFB, MA 01731. This will assist us in maintaining a current mailing list.

Do not return copies of this report unless contractual obligations or notices on a specific document requires that it be returned.

Unclassified

SECURITY CLASSIFICATION OF THIS PAGE (When Data Entered)

# REPORT DOCUMENTATION PAGE

READ INSTRUCTIONS BEFORE COMPLETING FORM

| | |
|---|---|
| 1. REPORT NUMBER: AFGL-TR-83-0314 | 2. GOVT ACCESSION NO. A145941 |
| 3. RECIPIENT'S CATALOG NUMBER | |
| 4. TITLE (and Subtitle): VECTOR MAGNETIC FIELD ANALYSIS OF LORENTZ FORCES ACTING IN THE SOLAR ATMOSPHERE. | 5. TYPE OF REPORT & PERIOD COVERED: Final Report 3 Dec 1981 - 31 July 1983 |
| | 6. PERFORMING ORG. REPORT NUMBER |
| 7. AUTHOR(s): K. KRALL, S. T. WU, J. B. SMITH, JR. | 8. CONTRACT OR GRANT NUMBER(s): F19628-82-K-0014 |
| 9. PERFORMING ORGANIZATION NAME AND ADDRESS: The University of Alabama in Huntsville, Huntsville, Alabama 35899 | 10. PROGRAM ELEMENT, PROJECT, TASK AREA & WORK UNIT NUMBERS: 61102F 2311G3CK |
| 11. CONTROLLING OFFICE NAME AND ADDRESS: Air Force Geophysics Laboratory, Hanscom AFB, Massachusetts 01731, Monitor/Donald F. Neidig/PHS | 12. REPORT DATE: 28 November 1983 |
| | 13. NUMBER OF PAGES: 42 |
| 14. MONITORING AGENCY NAME & ADDRESS (if different from Controlling Office) | 15. SECURITY CLASS. (of this report): Unclassified |
| | 15a. DECLASSIFICATION/DOWNGRADING SCHEDULE |

16. DISTRIBUTION STATEMENT (of this Report)

Approved for public release; distribution unlimited

17. DISTRIBUTION STATEMENT (of the abstract entered in Block 20, if different from Report)

18. SUPPLEMENTARY NOTES

19. KEY WORDS (Continue on reverse side if necessary and identify by block number)

Solar magnetic fields
Lorentz force calculations
Energy Buildup
Photospheric measurements
Flares

20. ABSTRACT (Continue on reverse side if necessary and identify by block number)

The role of magnetic fields during the energy storage and release process of the solar chromosphere/corona is addressed in the absence of detailed chromospheric field measurements. The potential utility of 3-component solar photospheric magnetic field measurements in determining the magnetic energy transfer to the overlying atmosphere is examined. Net Lorentz forces and torques exerted on the volume above the photospheric plane are determined for a specific MSFC Vector Magnetograph measurement set. Twenty-four hour trends during photospheric magnetic simplification appear consistent with a decline in energy

DD FORM 1473, 1 JAN 73 EDITION OF 1 NOV 65 IS OBSOLETE
S/N 0102-LF-014-6601

UNCLASSIFIED

SECURITY CLASSIFICATION OF THIS PAGE (When Data Entered)

transfer to the chromosphere. Noise within the data is found to be insignificant, while calibration uncertanties are large. An algorithm listing is provided. Keywords: Solar Flares, and Energy buildup.

TABLE OF CONTENTS

## 1. INTRODUCTION

Evaluating the role of electric currents in the energy storage process within coronal and chromospheric magnetic fields has been limited mainly to comparing field lines extrapolated from observed longitudinal photospheric values to emission features assumed to be field-aligned ( Tanaka and Nakagawa, 1973; Hagyard, 1976; Levine, 1976; Krall, et. al., 1978). These calculations have been done using arbitrary and overly simplistic constant-$\alpha$ ( = $\mu_o \underline{J}/\underline{B}$, where $\underline{J}$ is the current density, $\underline{B}$ the magnetic field, and $\mu_o$ the permeability in free space) assumptions concerning current distributions. Measuring the transverse component of the photospheric field allows a unique opportunity to obtain information about $\alpha$-distribution and thus the Lorentz forces exerted on the overlying layers. Unfortunately, utilizing an observationally deduced $\alpha$-distribution to compute the force-free field in the region above the observing plane is in general an intractable, nonlinear boundary value problem. However, a method exists for determining net Lorentz forces and magnetic energy within a force-free region without explicit solution of the field equations (eg. Molodensky, 1974). The purpose of this paper is to examine the utility of such a method, within the limitations of available vector magnetic field observations, in determining energy exchange between photospheric fields and the overlying atmosphere. Such a method may be potentially useful in real time for identifying modes and levels of energy buildup in the preflare active region.

A discussion of pertinent equations is presented in Section 2. In order to properly evaluate the results, measurement and calibration uncertainties are discussed in sections 3 and 4. Although the interpretation

of transverse measurements is subject to significant uncertainty, correlative observations may be utilized to test the integrity and resultant conclusions of the measurements (e.g., photospheric proper motion may be found to be consistent with generation of the $\underline{J} \times \underline{B}$ forces inferred from the measured fields). Section 5 presents application of the previously discussed formalism to two sets of Marshall Space Flight Center Vector Magnetograph data, a flare productive and migrating delta-configuration spot on 6 April 1980 and a large but rather simple (beta-gamma) region on 15-16 September 1980.

## 2. Theoretical Formulation

The vector sum of all electromagnetic forces acting within a volume V above the photosphere can be written as:

$$\underline{F} = \frac{1}{c} \int_V \underline{J} \times \underline{B} \, dV \tag{2-1}$$

where c is the velocity of light and we assume electric fields to play a negligible role due to the high electrical conductivity. Using Maxwell's equations

$$\underline{J} = \frac{c}{4\pi} \left( \underline{\nabla} \times \underline{B} \right) \tag{2-2}$$

and $$\underline{\nabla} \cdot \underline{B} = 0 \, , \tag{2-3}$$

Equation (2-1) can be written

$$\underline{F} = \int_V \frac{1}{4\pi} \left[ (\underline{\nabla} \times \underline{B}) \times \underline{B} + \underline{B} \, (\underline{\nabla} \cdot \underline{B}) \right] dV$$

$$= \int_V \frac{1}{4\pi} \left[ (\underline{B} \cdot \underline{\nabla})\underline{B} - \frac{1}{2} \nabla B^2 + \underline{B}(\underline{\nabla} \cdot \underline{B}) \right] dV \, . \tag{2-4}$$

The integral in Equation (2-4) can be identified as the divergence of the second rank Maxwell's stress tension $\overleftrightarrow{T}$,

$$\overleftrightarrow{T} = \frac{1}{4\pi} (\underline{B} \cdot \underline{B} - \frac{1}{2} \overleftrightarrow{I} B^2) \tag{2-5}$$

whose elements are

$$T_{ij} = \frac{1}{4\pi} \left\{ B_i B_j - \frac{1}{2} \delta_{ij} B^2 \right\} \tag{2-6}$$

where

$$\begin{aligned} \delta_{ij} &= 1 \qquad i = j \\ &= 0 \qquad i \neq j \, . \end{aligned} \tag{2-7}$$

Thus, the volume integral Equation (2-4) can be replaced by an integral over the surface S containing V:

$$\begin{aligned} F &= \int_V \underline{\nabla} \cdot \overleftrightarrow{T} \, dV \\ &= \int_S \underline{n} \cdot \overleftrightarrow{T} \, dS \end{aligned} \tag{2-8}$$

where $\underline{n}$ is the outward direction unit normal to S. In a similar fashion, the net electromagnetic torque $\underline{\tau}$ acting within a volume can be shown to be

$$\begin{aligned} \underline{\tau} &= \frac{1}{c} \int_V \underline{r} \times (\underline{J} \times \underline{B}) \, dV \\ &= \int_V \underline{r} \times (\underline{\nabla} \cdot \overleftrightarrow{T}) \, dV \\ &= \int_S \underline{n} \cdot (\overleftrightarrow{T} \times \underline{r}) \, dS \end{aligned} \tag{2-9}$$

where $T_{ij} = T_{ji}$ is used to arrive at Equation (2-9) and $\underline{r}$ is the position vector of a lever arm. Thus, if a volume enclosing chromospheric coronal

fields is appropriately chosen to give zero contribution to Equations (2-8) or (2-9) on all but the photospheric surface, a complete specification of $\underline{B}$ on that level is sufficient to determine a lower limit (net) to the magnetic forces or torques exerted on the volume. The work done by the photospheric fields and any resulting magnetic energy buildup cannot, of course, be determined by this method. In the absense of chromospheric or coronal magnetic field data, these can only be inferred indirectly (e.g. by changing fibril structure or energy release).

The net forces and torques, and total magnetic energy (which is derived similarly) can be expressed in Cartesian coordinates using longitudinal (z direction) and transverse (x-y plane) field measurements.

horizontal force $$F_x = \frac{-1}{4\pi} \sum_{x,y} B_z \cdot B_x \cdot \Delta S$$

and $$F_y = \frac{-1}{4\pi} \sum_{x,y} B_z \cdot B_y \cdot \Delta S, \qquad (2\text{-}10)$$

vertical force $$F_z = \frac{-1}{8\pi} \sum_{x,y} \left(B_z^2 - B_x^2 - B_y^2\right) \cdot \Delta S, \qquad (2\text{-}11)$$

torque about a vertical axis $$\tau = \frac{1}{4\pi} \sum_{x,y} B_z \left(B_x \cdot \Delta y - B_y \cdot \Delta x\right) \cdot \Delta S, \qquad (2\text{-}12)$$

and energy $$E = \frac{1}{4\pi} \sum_{x,y} B_z \left(B_x \cdot \Delta x + B_y \cdot \Delta y\right) \cdot \Delta S. \qquad (2\text{-}13)$$

## 3. Measurements

The MSFC Vector Magnetograph utilizes a .125Å Zeiss filter, tunable to 10 mÅ increments within the FeI 5250.2Å line. All observations discussed here are centered at $\lambda$ = 60, 90 or 120 mÅ in the blue wing of that line. The measured components of the magnetic field are assumed to be

$$B_z = k\, C_1(\Delta\lambda)\, P_V(\Delta\lambda) \tag{3-1}$$

$$B_T = \left(B_x^2 + B_y^2\right)^{1/2} = k^{1/2}\, C_2(\Delta\lambda)\, P_Q(\Delta\lambda) \tag{3-2}$$

where the fractional circularly-polarized intensity

$$P_V = \left(I_1 - I_2\right) \Big/ \left(I_1 + I_2\right), \tag{3-3}$$

and linearly polarized intensity

$$P_Q = \left(U^2 + R^2\right)^{1/2} \tag{3-4}$$

and

$$U = \left(I_3 - I_4\right) \Big/ \left(I_3 + I_4\right), \quad R = \left(I_5 - I_6\right) \Big/ \left(I_5 + I_6\right) \tag{3-5}$$

are functions of the MSFC Vector Magnetograph raw intensity counts described in Table I. The direction $\phi$ of the tranverse field where

$$B_x = B_T \cos\phi$$

and

$$B_y = B_T \sin\phi, \tag{3-6}$$

is found as

$$\phi = .5 \tan^{-1} (U/R). \tag{3-7}$$

The values for $C_1$, $C_2$ were determined from theoretical calibration curves derived from the Kjeldseth Moe solutions to the radiative transfer equations (Kjeldseth Moe, 1968) for penumbral and umbral atmospheric models. The parameter k represents a scaling factor which adjusts measured polarization for loss of contrast and was determined by scaling the maximum B magnitude with that of Mt Wilson measurements. Corrections for linear and circular crosstalk in the MSFC data are discussed in the following paragraphs.

Average background (quiet sun) measurements of $P_V$ and $P_Q$ are normally used to look for linear and circular polarization biases. Typically, no circular bias is present; however, random linear polarization biases are found and are attributed to the magnetograph's correlation tracker subsystem. Figure 1 a-d shows an example of the distribution of weak field polarization values used in determining these biases. Figure 2 a-d shows corresponding distributions after correcting for bias.

Circular crosstalk, the effect of coupling circular into linear polarization measurements in strong field areas, must also be considered in the calibration process to eliminate biasing $\phi$. Figure 3 a,b are scatter plots of U and R vs $P_Q$, with the linear least squares fits showing the artificial correlation induced by crosstalk. A correction factor has been introduced in Figure 4 a,b to eliminate the correlation.

## 4. Error Analysis

The effects of signal to noise and calibration must be estimated in order to determine the integrity of the measurements. This section describes the treatment of noise in the linear and circular polarization measurements used to derive longitudinal and transverse fields.

The physical parameters to be evaluated are Equations (2-10) through (2-13) and direction of horizontal force:

$$\theta = \tan^{-1}\left(\frac{F_y}{F_x}\right) .$$

Gaussian statistics are used to determine the standard deviation at each pixel i,j:

$$\left(\sigma_\tau^2\right)_{ij} = \left\{B_z^2\left(\Delta y^2\sigma_{B_x}^2 + \Delta x^2\sigma_{B_y}^2\right) + \sigma_{B_z}^2\left(\Delta y\ B_x - \Delta x\ B_y\right)^2\right\}\Delta S^2, \quad (4\text{-}1)$$

$$\left(\sigma_E^2\right)_{ij} = \left\{B_z^2\left(\Delta x^2\sigma_{B_x}^2 + \Delta y^2\sigma B_y^2\right) + \sigma_{B_z}^2\left(\Delta x\ B_x + \Delta y\ B_y\right)^2\right\}\Delta S^2, \quad (4\text{-}2)$$

$$\left(\sigma F_x\right)_{ij} = \left\{B_z^2\ \sigma_{B_x}^2 + B_x^2\ \sigma_{B_z}^2\right\}\ \Delta S^2,$$

$$\left(\sigma F_y\right)_{ij} = \left\{B_z^2\ \sigma_{B_z}^2 + B_y^2\ \sigma_{B_z}^2\right\}\Delta S^2,$$

$$\left(\sigma F_z^2\right)_{ij} = 4\left(B_z^2\ \sigma_{B_z}^2 + B_x^2\ \sigma_{B_x}^2 + B_y^2\ \sigma_{B_y}^2\right)\ \Delta S^2, \quad (4\text{-}3)$$

$$\sigma_\theta^2 = \left[\frac{1}{1 + (F_y/F_x)^2}\right]^2\left[\frac{1}{F_x^2}\ \sigma_{F_y}{}^2 + \frac{F_y^2}{F_x^4}\ \sigma_{F_x}{}^2\right] . \quad (4\text{-}4)$$

Equations 3-1 through 3-9 are used to determine the field uncertainties:

$$\sigma_{B_z}^2 = \left(2C_1 k\right)^2 \left(\sigma_{I_1}^2 I_2^2 + \sigma_{I_2}^2 I_1^2\right) \Big/ \left(I_1 + I_2\right)^4 \tag{4-5}$$

$$\sigma_{B_x}^2 = \sigma_{B_T}^2 \cos^2 \phi + B_T^2 \sum_{i=3,6} \left(\frac{\partial \cos \phi}{\partial I_i}\right)^2 \sigma_{I_i}^2 \tag{4-6}$$

$$\sigma_{B_y}^2 = B_T^2 \sin^2 \phi + B_T^2 \sum_{i=3,6} \left(\frac{\partial \sin \phi}{\partial I_i}\right)^2 \sigma_{I_i}^2 \tag{4-7}$$

where

$$\sigma_{B_T} = C_2^2 K \left(U^2 \sigma_U + V^2 \sigma_R\right) \Big/ 4 \left[U^2 + R^2\right]^{3/2} \tag{4-8}$$

and

$$\frac{\partial \cos \phi}{\partial I_3} = - \left[\frac{.5}{1 + x^2}\right] \frac{2 I_4 R^{-1}}{(I_3 + I_4)^2} \sin \phi$$

$$\frac{\partial \cos \phi}{\partial I_4} = \left[\frac{.5}{1 + x^2}\right] \frac{2 I_3 R^{-1}}{(I_3 + I_4)^2} \sin \phi$$

$$\frac{\partial \cos \phi}{\partial I_5} = \left[\frac{.5}{1 + x^2}\right] \frac{U}{R^2} \frac{2 I_6}{(I_5 + I_6)^2} \sin \phi$$

$$\frac{\partial \cos \phi}{\partial I_6} = \left[\frac{.5}{1 = x^2}\right] \frac{U}{R^2} \frac{2 I_5}{(I_5 + I_6)^2} \sin \phi$$

$$\frac{\partial \sin \phi}{\partial I_i} = \frac{\partial \cos \phi}{\partial I_i} \operatorname{ctn} \phi \quad . \tag{4-9}$$

Appendix A lists the algorithm developed during this effort and used

on MSFC data to calculate Equations 2-10 through 2-13 and $\theta$, as well as standard deviations 4-1 through 4-4. Input from data files are raw intensitites $I_1$ through $I_6$ and processed fields $B_z$, $B_x$, $B_y$ (i.e., after calibrations and elimination of the 180° ambiguity in transverse field direction).

The standard deviation in the raw data ($\sigma_{I_i}$) produces the spread in the zero-field distributions ($\sigma_{P_Q}$ and $\sigma_{P_V}$) in Figure 2. Equations 4-5 through 4-7 can therefore also be written in terms of measured $\sigma P_Q$ and $\sigma_{P_V}$, and are written so within the present code.

## 5. Results

In an earlier calculation (Krall, et al. 1982), a small, migrating and flare producing portion of Boulder SESC AR2372 (Figure 5) was evaluated using the equations of Section 2.

For the 48 hour period containing the maximum photospheric proper motion and flare activity, Figure 6 shows the direction of horizontal magnetic force for the area containing the small westward moving positive spot. The calculated force was directed within 30 degress of the observed motion of the spot during the time of maximum spot motion and flare activity, changing significantly (and decreasing somewhat) outside of that time period. This is as expected if the photospheric motions act to magnetically transfer forces to the overlying atmosphere. Such forces can of course be dissipated rapidly or stored in a higher energy magnetic configuration. The later possibility is more likely here due to the high flare activity of the period.

Although AR2372 was an extremely interesting region from the viewpoint of this analysis, several factors combined to complicate the interpretation:

1. There are possibly strong field saturation effects.
2. Region complexity made difficult the task of eliminating the 180 degree ambiguity in the direction of the tranverse field component.
3. Inadequate observations at greater than 60 mÅ from the line center increased the possibility of magneto-optical effects (West and Hagyard, 1983).
4. There was insufficient time resolution for an analysis of magnetic energy buildup or dissipation for such a rapidly evolving region (During the period an M or X class flare occurred on the average every 5 hours and C class flare every 8 hours).

It was therefore decided that a region of less spatial and temporal complexity was needed to properly evaluate the potential of this type of analysis. Boulder SESC # AR2665 (Figure 7), a simple large spot region on its second disk transit, was well observed at 90 and 120 mÅ on September 15 and 16, had little indication of saturation at those wavelengths, and was by its single spot nature, relatively easy to treat for its transverse field direction ambiguity. Its most significant characteristics were a large leader spot (of positive polarity) and a lack of pronounced magnetic complexity.

During the first few days of its rotation across the visible disk, AR2665 did exhibit some complexity and some evidence of sheared $B_T$ fields, and produced several relatively small flares near the weakly sheared neutral line. Flare history (Figure 8) and magnetic history (Figure 9) both reached maxima from September 11 - 13.

The region had been simplifying, and continued to simplify during the period of interest. Between 15/1349UT and 16/1359UT (Figure 7a and c) the $B_L$ gradients along the neutral line had decreased, the field strengths (both $B_L$ and $B_T$) had declined near the neutral line, and the $B_T$ configuration had become more potential appearing (orthogonal to the $B_L = 0$ line) in orientation.

The more frequent flare activity occurred before the times of the Lorentz force evaluation (Figure 8), with only one C1 and 2 subflares without associated x-rays occurring during the 72 hours after the beginning of the analysis. AR2665 had been reported as a beta-gamma region (somewhat magnetically complex) but by the 15th, observations of the magnetic field indicated it to be a simple beta (simple bipole) magnetic configuration.

Figure 10 shows physical parameters (Equations [2-11] through [2-13] for a 24 hour period during the decay of region AR 2665. Points to be emphasized are:

1. Signal to noise is seen in all cases to be small compared to time variation and observing wavelength variation.

2. Although wavelength variation is only available at one time point in Figure 10 (actually a twenty minute period at 2000 UT on 15 September), the results are consistent with a measurement degradation as one approaches line center, e.g., a negative vertical force at 60 mÅ requires unlikely submerging magnetic flux or upward counter-forces. Such degradation is consistent with magneto-optical effects; in fact, detailed analysis for this region shows that reliable transverse field directions may be obtainable only at $\Delta\lambda \geq 120$ mÅ (West and Hagyard, 1983). In addition, the tightening spiral configuration suggested by the divergence in torque with decreasing observation wavelength is also consistent with magneto optical effects.

3. In the declining phase of AR 2665, available energy is seen to decay by $10^{32}$ ergs/day. If this is not an observational effect, significant energy release over a relatively short time period ($10^{32}$ ergs/few hours) might be claimed to have been observed.

4. Upward vertical force decreases during the 24 hours; this could be interpreted as a declining rate of emerging flux. A declining, yet always positive rate of emerging flux is to be expected during the demise of an active region. (This upward energy flux would be more than compensated for by dissipative processes during the decay phase, whereas the converse would be true during region growth.)

## 6. Concluding Remarks

We have developed and utilized a procedure for evaluating the potential role of 3-component photospheric magnetic field measurements for studying the magnetic energy buildup process within solar active regions. We have applied the equations to two regions and the results appear encouragingly consistent with expectations, both as a function of time (physical variations) and wavelength (observational variations). Further evidence is presented that these type observations must be made at or greater than 90 mÅ from line center.

Important questions as yet to be answered during the validation process are:

1. Does the measured vertical magnetic force increase during early active region growth (when emerging flux is most apparent), reach a maximum, and then decay within the proper time frame? This is probably not answerable within the lifetime of single active regions, but can be approached by studying regions in each phase of growth.

2. Do proper spot motions (or rotations) show up as increased horizontal magnetic force (torque), and can these motions now be more quantitatively linked to magnetic energy buildup and release?

# 7. Appendix: Algorithm Listing

```
C       THIS PROGRAM CALCULATES THE 3 COMPONENTS OF NET FORCE, TORQUE,
C       ENERGY AND THE SIGNAL/NOISE UNCERTAINTIES ASSOCIATED WITH THEM
C       INPUT FROM TAPE 9 IS THE OBSERVED PHOTOSPHERIC BX,BY AND BZ
C       INPUT FROM TAPE 10 IS I1,I2,...I6 RAW DATA CORRESPONDING TO FIELD
C        STRENGTHS FROM TAPE 9
        DIMENSION SIGT(41,41),SIGE(41,41),B(3,41,41),IR(6),AM(10)
        DIMENSION F(3),YORIGN(10),XORIGN(10)
        DIMENSION         C1OLD(6),C1NEW(6),C2OLD(6),C2NEW(6)
        DIMENSION BTPHI(41,41)
        REAL KNEW(6)
        REAL KOLD(6)
        REAL  IT(6,41,41)
        REAL  KFACT
        REAL  I56,I34,I56P,I34P,I12,I12P
C
C
        DATA YORIGN/19.,16.,16.,19.,15.,5*.0/
        DATA XORIGN/25.,23.,24.,23.,25.,5*0./
C
C
        DATA IR/1,2,3,4,5,0/
C       UMBRAL MODEL
        DATA C1NEW/4374.,2707.,3195.,4374.,4374.,0./
        DATA C1OLD/6690.,3182.,4311.,6690.,6690.,0./
        DATA C2NEW/3628.,2568.,2910.,3628.,3628.,0./
        DATA C2OLD/4437.,2591.,3191.,4437.,4437.,0./
        DATA KNEW  /7.18,9.16,8.56,7.03,6.72,0./
        DATA KOLD /4.7,7.8,6.35,4.6,4.4,0./
        DATA AM/1.,0.,0.,1.,0.,0.,4*0./
        DS=2.5*725E5
        PI=3.14159
        DTOR=PI/180.
C       MAX PI/2 UNCERTAINTY IN DIRECTION
        SPHIMX=PI/2.
        FRPI=4.*PI
C       DEFINE SIGPQ, SET INITIAL GUESS ON SIG3**2
        SIGPQ=.001
        SIG32=170.
C
C
        DO 10 KTAPE1=1,6
C
C
C       INITIAL TIME FOR FINDING INTENSITY VARIANCES,SUCEEDING TIMES FOR
C       CALC PHYSICAL SIGMAS
        KTAPE=KTAPE1
        IF(KTAPE1.GT.1) KTAPE=KTAPE1-1
        IF(KTAPE.EQ.1) REWIND9
C       RESET VARIABLES
        GO TO 100
  109   CONTINUE
C       READ DATA
        GO TO 120
  129   CONTINUE
C       LOOP THROUGH DATA ARRAY, CALCULATING UNCERTAINTIES
        GO TO 140
  149   CONTINUE
```

```
C
      DTDFY=F(2) / (F(2)**2 + F(3)**2)
      DTDFX=-F(3) / (F(2)**2 + F(3)**2)
      TAUTOT=TAU/TAUTOT
      ETOT=EN/ETOT
      FXTOT=F(2)/FXTOT
      FYTOT=F(3)/FYTOT
      TAU=TAU*DS*DS*DS/FRPI
      EN=EN*DS*DS*DS/FRPI
      DO 2 I=1,3
    2 F(I)=F(I)*DS*DS/FRPI
      FHMAG=SQRT(F(2)*F(2) + F(3)*F(3))
C     ROTATE BACK TO X-Y COORDS
C     FX=F(2)*COS(20.*DTOR)-F(3)*SIN(20.*DTOR)
C     F(3)=F(2)*SIN(20.*DTOR)+F(3)*COS(20.*DTOR)
C     F(2)=FX
      THETA=F(3)/F(2)
      THETA=ATAN(THETA)/DTOR
      IF(ITP.EQ.0) GO TO 9
      SIGTH2=SIGFX*DTDFX**2 + SIGFY*DTDFY**2
      SIGDEG=SQRT(SIGTH2)/DTOR
      SIG32P= SIGPQ * SIGPQ * (ISTOP-ISTART+1) * (JSTOP-JSTART+1)/DPQDI2
      IF(KTAPE1.EQ.1) SIG32=SIG32P
      SIGT(IO,JO)=SQRT(SIGT(IO,JO))*DS*DS
      SIGE(IO,JO)=SQRT(SIGE(IO,JO))*DS*DS*DS/FRPI
      SIGFZ=SQRT(SIGFZ)*DS*DS/FRPI
      SIGFX=SQRT(SIGFX)*DS*DS/FRPI
      SIGFY=SQRT(SIGFY)*DS*DS/FRPI
9     CONTINUE
      WRITE(6,6)
6     FORMAT(///,50H  TORQUE     ENERGY      FZ         FX         FY    )
      WRITE(6,7) TAU,EN,(F(I),I=1,3)
      WRITE(6,7) SIGT(IO,JO),SIGE(IO,JO),SIGFX,SIGFY,SIGFZ
      WRITE(6,7) TAUTOT,ETOT,FXTOT,FYTOT ,FHMAG
      WRITE(6,8) SIGDEG,SIG32,SIG32P,THETA,SIGPQ
8     FORMAT(//
     $        14H SIGMA THETA= ,E10.3,25H D   SIGMA INTENSITY USED,E10.3,
     $25H     SIGM INTENSITY CALC=,E10.3,10H    THETA=,F5.1,
     $12H     SIGM PQ=,E8.2)
7     FORMAT(5E10.3)
10    CONTINUE
      STOP
C                   * * * *  B L O C K  1 0 0  * * * *
C                                                                  (BLKC)
C     INITIALIZE VARIABLES
C
100   CONTINUE
C     RESET VARIABLES
      ITP=IR(KTAPE)
      WRITE(6,103)
103   FORMAT(1H1)
      WRITE(6,102)  KTAPE,ITP
102   FORMAT(2I10)
      SIG12=SIG32
      SIG22=SIG32
      SIG42=SIG32
      SIG52=SIG32
```

```
      SIG62=SIG32
C     IKNOWN=0 FOR K ONLY KNOWN, 1 FOR K,C1,C2 KNOWN
      IKNOWN=1
      KFACT=KNEW(KTAPE)
C     KFACT=4.
C     C1=1000.
C     C2=1000.
      C1=C1NEW(KTAPE)
      C2=C2NEW(KTAPE)
      JO=XORIGN(KTAPE)
      IO=YORIGN(KTAPE)
      TAU=0.
      EN=0.
      SIGT(IO,JO)=0.
      SIGE(IO,JO)=0.
      SIGFX=0.
      SIGFY=0.
      SIGFZ=0.
      SIGQ2=0.
      DPGDI2=0.
      DO 101 I=1,3
  101 F(I)=0.
      THETA=0.
      SIGTH2=0.
      ETOT=0.
      TAUTOT=0.
      FXTOT=0.
      FYTOT=0.0
      GO TO 109
C                   * * * *  B L O C K  1 2 0  * * * *
C                                                                 (BLKC)
120   CONTINUE
C
C     READ DATA FILES
      READ(9) M,N,(((B(K,I,J),J=1,N),I=1,M),K=1,3)
C
C
C
      WRITE(6,124)
124   FORMAT(1H1)
      WRITE(6,123)((B(1,I,J),J=1,39,2),I=1,39,2)
123   FORMAT(20F6.0)
      DO 125 I=1,M
      DO 125 J=1,N
      BTPHI(I,J)=ATAN(B(3,I,J)/B(2,I,J))/DTOR
      IF(B(3,I,J).LT.0..AND.B(2,I ,J).LT.0.) BTPHI(I,J)=BTPHI(I,J)-180.
      IF(B(3,I,J).GT.0..AND.B(2,I ,J).LT.0.) BTPHI(I,J)=BTPHI(I,J)+180.
125   CONTINUE
      WRITE(6,124)
      WRITE(6,123)((BTPHI(I,J),J=1,39,2),I=1,39,2)
      WRITE(6,124)
C
C
C
      REWIND 10
      IF(ITP.EQ.0) GO TO 122
      DO 121 ITAPE=1,ITP
```

```
      IF(AM(ITP).EQ.1.) READ(10)(((IT(K,I,J),I=M,1,-1),J=N,1,-1),K=1,6)
      IF(AM(ITP).EQ.0.) READ(10)(((IT(K,I,J),I=1,M),J=1,N),K=1,6)
  121 CONTINUE
122   CONTINUE
      GO TO 129
C                 * * * *  B L O C K   1 4 0  * * * *
C                                                                (BLK0)
140   CONTINUE
C     LOOP THROUGH DATA ARRAY
C
      ISTOP=M
      JSTART=1
      JSTOP=N
      ISTART=1
      ICHK=ISTART+3
      JCHK=JSTART+3
C     RECOVER RAW DATA
      DO 141 I=1,M
      DO 141 J=1,N
      DO 141 KCAL=1,6
  141 IF(IT(KCAL,I,J).LT.0.) IT(KCAL,I,J)=IT(KCAL,I,J)+65536.
C
C
C     USE CORRECT OR UPDATED CONSTANTS
C
C
      COR1=1.
      COR2=1.
C
C
      COR2=SQRT(KNEW(ITP)/KOLD(ITP))*C2NEW(ITP)/C2OLD(ITP)
      COR1=KNEW(ITP)*C1NEW(ITP)/(KOLD(ITP)*C1OLD(ITP))
C
C
      DO 148 I=ISTART,ISTOP
      DI=I-I0
      DO 147 J=JSTART,JSTOP
      DJ=J-J0
      B(1,I,J)=B(1,I,J)*COR1
      B(2,I,J)=B(2,I,J)*COR2
      B(3,I,J)=B(3,I,J)*COR2
      BX= B(2,I,J)
      BY=B(3,I,J)
      BZ=B(1,I,J)
C
C
C     CALCULATE PHYSICALS
      GO TO 1000
 1009 CONTINUE
C
C     CORRECT SIGNS OF B IF NECESSARY( Y UP,BX TO RIGHT,BZ OUT OF PLANE)
      BX=-(B(2,I,J)*COS(20.*DTOR)+B(3,I,J)*SIN(20.*DTOR))
      BY=- B(2,I,J)*SIN(20.*DTOR)+B(3,I,J)*COS(20.*DTOR)
      BZ=B(1,I,J)
      BT=SQRT(BX*BX+BY*BY)
      IF(ITP.EQ.0) GO TO 147
C
```

```
C      IF CALIBRATION CONSTANTS NOT KNOWN, CALCULATE THEM
C
       IF(IKNOWN.EQ.0.AND.I.EQ.ISTART.AND.J.EQ.JSTART) GO TO 1010
 1019  CONTINUE
C      CALCULATE INTENSITY DIFFERENCES,SUMS
       I56= IT(5,I,J)-IT(6,I,J)
       I56P=IT(5,I,J)+IT(6,I,J)
       I34= IT(3,I,J)-IT(4,I,J)
       I34P= IT(3,I,J)+IT(4,I,J)
       I12= IT(1,I,J)-IT(2,I,J)
       I12P= IT(1,I,J)+IT(2,I,J)
C      CALCULATE U,V,SIGU,SIGV
       U= I34/I34P
       V= I56/I56P
       UVMAG=U*U+V*V
       U2V2= (U/I34P)**2 + (V/I56P)**2
C      DPQDI2=DPQDI2 + 2.*KFACT*KFACT*U2V2 / (U*U+V*V)
       DPQDI2=DPQDI2 + 2.    *          U2V2 / (U*U+V*V)
       SIGU= (1.-U)**2 * (SIG32 + SIG42)/(I34P*I34P)
       SIGV= (1.-V)**2 * (SIG52 + SIG62)/(I56P*I56P)
C      IF(KTAPE.EQ.4)
C     $WRITE(6,144) I56,I56P,I34,I34P,I12,I12P,U,V,UVMAG,U2V2,SIGU,SIGV
144    FORMAT (12E10.3)
C
C      DETERMINE DIRECTION PARAMETERS
       GO TO 1020
 1029  CONTINUE
C      GO TO 1050
C1059  CONTINUE
C      CALCULATE B SIGMAS
       GO TO 1030
 1039  CONTINUE
C      CALCULATE PARAMETER SIGMAS, CHECK FOR LARGE TERMS
       GO TO 1040
 1049  CONTINUE
  147  CONTINUE
  148  CONTINUE
       GO TO 149
C                 * * * *  B L O C K  1 0 0 0  * * * *
C                                                               (BLK 140)
1000   CONTINUE
C
C      CALCULATE FORCES,ETC.
C      TORQUE = BZ * (BX * DY -BY*DX)
       T=BZ*(BX*DI-BY*DJ)
       E=BZ* (BX*DJ + BY*DI)
       F1=BZ*BZ-BX*BX-BY*BY
       F2=BZ*BX
       F3=BZ*BY
C      SUM OVER ARRAY
       EN=EN+E
       TAU=TAU+T
       F(1)=F(1)+F1
       F(2)=F(2)+F2
       F(3)=F(3)+F3
       ETOT=ETOT+ABS(E)
       TAUTOT=TAUTOT+ABS(T)
```

```
      FXTOT=FXTOT+ABS(F2)
      FYTOT=FYTOT+ABS(F3)
      GO TO 1009
C                 * * * *  B L O C K  1 0 1 0  * * * *
C                                                                (BLK 140)
1010  CONTINUE
      IFLAG=0
      VAR1=0.
      VAR2=0.
1015  CONTINUE
C
C     CALCULATE C1,C2,GIVEN KFACT
      ICOUNT=0
      JCOUNT=0
      RATIO1=0.
      RATIO2=0.
      BLIM=500.
      PLIM=10.
      DO 1018 I10=1,M
      DO 1017 J10=1,N
        BZC=B(1,I10,J10)
      IF(BZC.LT.BLIM.AND.BZC.GT.-BLIM) GO TO 1011
      BZP= KFACT *
     1    (IT(1,I10,J10)-IT(2,I10,J10))/(IT(1,I10,J10)+IT(2,I10,J10))
      RAT1=BZC/BZP
      IF(IFLAG.EQ.1) VAR1=VAR1+(RAT1-C1)**2
C     WRITE(6,9011)I10,J10,RAT1,BZC,BZP,IT(1,I10,J10),IT(2,I10,J10)
C9011 FORMAT(2I5,7F10.3)
      RATIO1=RATIO1+BZC/BZP
      ICOUNT=ICOUNT+1
 1011 CONTINUE
      BTC=SQRT(B(2,I10,J10)**2+B(3,I10,J10)**2)
      IF(BTC.LT.BLIM.AND.BTC.GT.-BLIM) GO TO 1012
      U=(IT(3,I10,J10)-IT(4,I10,J10))/(IT(3,I10,J10)+IT(4,I10,J10))
      V=(IT(5,I10,J10)-IT(6,I10,J10))/(IT(5,I10,J10)+IT(6,I10,J10))
      UVMAG=U*U+V*V
      BTP= SQRT(KFACT*SQRT(UVMAG))
      RATIO2=RATIO2+BTC/BTP
      RAT2=BTC/BTP
      IF(IFLAG.EQ.1) VAR2=VAR2+(RAT2-C2)**2
C     WRITE(6,9011)I10,J10,RAT2,BZC,BZP,IT(3,I10,J10),IT(4,I10,J10),
C    $                                  IT(5,I10,J10),IT(6,I10,J10)
      JCOUNT=JCOUNT+1
 1012 CONTINUE
 1017 CONTINUE
 1018 CONTINUE
      C1P = RATIO1/(ICOUNT*1.)
      C2P=RATIO2/(JCOUNT*1.)
      WRITE(6,1013) KFACT,C1,C1P,C2,C2P,IKNOWN
 1013 FORMAT(3X, 6H K =  ,F5.2,13H  C1(GIVEN)= ,F6.0,13H  C1(CALC)=
     $F6.0,13H  C2(GIVEN)= ,F6.0,13H  C2(CALC)=  ,F6.0,10H IKNOWN=  ,I5)
      IF(IKNOWN.EQ.1) GO TO 1014
      C1=C1P
      C2=C2P
 1014 CONTINUE
      IF(IFLAG.EQ.1) VAR1=SQRT(VAR1)/ICOUNT
      IF(IFLAG.EQ.1) VAR2=SQRT(VAR2)/JCOUNT
```

```
      IFLAG=IFLAG+1
      IF(IFLAG.LT.2) GO TO 1015
                        WRITE(6,1016) VAR1,VAR2
1016  FORMAT(2E10.3)
      GO TO 1019
C                 * * * *  B L O C K  1 0 2 0  * * * *
C                                                                (BLK 140)
1020  CONTINUE
C
C     CALCULATE DIRECTION, DIRECTION VARIANCE
      PHI=ATAN(BY/BX)
      CHI=-TAN(2.*PHI)
      DENOM=(I34/I56)*(I56P/I34P)
      DFACT=.5/(1. + DENOM*DENOM)
      DPD3= 2.*DFACT * IT(4,I,J)*I56P/(I34P*I34P*I56 )
      DPD4= 2.*DFACT * IT(3,I,J)*I56P/(I34P*I34P*I56 )
      DPD5= 2.*DFACT * IT(6,I,J)*I34 /(I56 *I56 *I34P)
      DPD6= 2.*DFACT * IT(5,I,J)*I34 /(I56 *I56 *I34P)
      SIGPHI =  SIG32*DPD3*DPD3
     $         + SIG42*DPD4*DPD4
     $         + SIG52*DPD5*DPD5
     $         + SIG62*DPD6*DPD6
      SIGPHI=SQRT(SIGPHI)
      IF(SIGPHI.GT.SPHIMX) SIGPHI=SPHIMX
      GO TO 1029
C                 * * * *  B L O C K  1 0 3 0  * * * *
C                                                                   (BLK 140)
1030  CONTINUE
C
C     CALCULATE B SIGMAS
      TA=  C2*C2*KFACT*(U*U*SIGU+V*V*SIGV)/(4.*UVMAG*SQRT(UVMAG))
      TB= (.5/(1.+CHI*CHI))**2.*(( SIG32+SIG42)/(I34*I34)
     $                            +(SIG52+SIG62)/(I56*I56) )
      TB=1.
      TC=SIGPHI*SIGPHI*BT*BT
      SIGBX2 = TA * COS(PHI)**2 + TC*TB*SIN(PHI)**2
      SIGBY2 = TA*SIN(PHI)**2 + TC*TB*COS(PHI)**2
      SIGBZ2=
     $4.*C1*C1*KFACT**2     * (SIG12*IT(2,I,J)**2 + SIG22*IT(1,I,J)**2)/
     $I12P**2/I12P**2
      GO TO 1039
C                 * * * *  B L O C K  1 0 4 0  * * * *
C
1040  CONTINUE
C     CALCULATE PARAMETER SIGMAS, CHECK FOR LARGE TERMS
      CHECK=.5
      ST= BZ*BZ*(DJ*DJ*SIGBX2 + DI*DI*SIGBY2)
     1 + SIGBZ2* (DJ*BX - DI*BY)**2
C     ST=   DJ*DJ * (BZ*BZ*SIGBX2  +  BX*BX*SIGBZ2)
C    $   +  DI*DI * (BZ*BZ*SIGBY2  +  BY*BY*SIGBZ2)
      SE=  (BX*DI+BY*DJ)**2*SIGBZ2  +  BZ*BZ*(SIGBX2*DI*DI+SIGBY2*DJ*DJ)
      SFX=  BZ*BZ*SIGBX2 + BX*BX*SIGBZ2
      SFY=  BZ*BZ*SIGBY2 + BY*BY*SIGBZ2
C
      SFZ= 4.*(BZ*BZ*SIGBZ2 + BX*BX*SIGBX2 + BY*BY*SIGBY2)
C
      IF(I.LT.ICHK.AND.J.LT.JCHK) GO TO 1041
```

```
      CHKT= SIGT(IO,JO) *CHECK
      CHKE= SIGE(IO,JO) *CHECK
      CHKX= SIGFX        *CHECK
      CHKY= SIGFY        *CHECK
      CHKZ= SIGFZ        *CHECK
      IF(CHKT.GT.ST  .AND.  CHKE.GT.SE .AND.  CHKX.GT.SFX .AND.
     $   CHKY.GT.SFY  .AND.  CHKZ.GT.SFZ ) GO TO 1041
      WRITE(6,1042)I,J,  ST,SE,SFX,SFY,SFZ,BX,BY,BZ
1042  FORMAT(2I5,36H FOLLOWING ARE T,E,FX,FY,FZ,VARIANCES,5E10.2,3F8.0)
      WRITE(6,1043) SIGT(IO,JO),SIGE(IO,JO),SIGFX,SIGFY,SIGFZ
1043  FORMAT(46H          AND RUNNING TOTALS ARE                  ,5E10.2)
1041  CONTINUE
      SIGT(IO,JO)=SIGT(IO,JO) + ST
      SIGE(IO,JO)=SIGE(IO,JO) + SE
      SIGFX= SIGFX + SFX
      SIGFY= SIGFY + SFY
      SIGFZ= SIGFZ + SFZ
      GO TO 1049
C   BLOCK 1050  $$$$
1050  CONTINUE
      PHI1=ATAN(-U/V)
      IF(V.LT.0.) PHI1=PHI1+PI
      PHI1=PHI1/(2.*DTOR)
      PHI=PHI/DTOR
      WRITE(6,1051) PHI,PHI1,I,J
      PHI=PHI*DTOR
1051  FORMAT(2F10.3,2I5)
C     GO TO 1059
      STOP
      END
```

## FIGURE CAPTIONS

Figure 1. Distribution of polarization measurements for weak field picture elements of solar active region 2665, used for determining observational biases and uncertainties. Normalized frequency of occurrence is plotted against (a-b) two components of linear polarization, (c) circular and (d) total linear polarization. If no biases have been introduced, distributions should center and peak at zero. Small biases in transverse measurements probably are induced by griding optics.

Figure 2. Distribution of polarization measurements (See Figure 1) after minor correction for biases. Spread in distribution ($\sigma_{P_V}$ and $\sigma_{P_Q}$) gives random uncertainties used in estimating noise effects.

Figure 3a-b. Circular Crosstalk Determination. The measured circular polarization is compared with the two components of the linear polarization, with each plotted point representing a picture element. Only the weak fields are shown and, therefore, the relationship of linear to circular polarization should be random. The weak but systematic correlation (seen here) between the magnitude of the circular and linear polarization measurements implies circular crosstalk into the linear polarization measurements. In the case shown, the deviation of best fit straight lines from horizontal approximates the degree (percentage) of crosstalk observed. Although an infrequent problem, crosstalk testing and correction procedures are routinely incorporated into the MSFC data analysis programs.

Figure 4a-b. Circular Crosstalk Correction. Same as Figure 3, after the estimated correction for percentage of circular crosstalk has been applied to the data. Linear polarization data now appear free of circular crosstalk influence. (Note that the best fit for the zero values approximates a horizontal line.)

Figure 5. Contours of circular polariztion measurements for AR2372 during the time of spot motions and greatest flare activity. In all figures, solid lines depict positive magnetic polarity, dashed lines are negative, and orientations are the same. Contours levels are $\pm$ 0.01, 1.0, 2.5, and multiples of $\pm$ 5% polarization.

Figure 6. Measured direction of horizontal force ($\theta$) for AR2372. Greatest spot migration occurred after data points on 5 April and before point on 7 April. Direction of proper motion of the migrating spot (from white light and magnetograms, Figure 5) agree well with data points on 6 April.

Figure 7. Vector Magnetographs of AR2665. The line-of-sight component ($B_L$) is represented by contours of field strength, solid for positive values and dashed for negative values. The transverse component ($B_T$) is represented by azimuthal vectors where length is proportional to field strength. The minimum length represents 300 Gauss and the maximum length represents 1000 Gauss. Note the changes occurring in the vicinity of the line of $B_L$ polarity reversal. Throughout the period under study, there is weakening of both $B_L$ and the $B_T$ components of the field. Continuing simplification is also shown by the increasing orthogonal nature (less shear) of the transverse component.

Figure 8. Histogram of X-ray Flares for AR2665. Logrithmic plot with C1 = $10^{-3}$ ergs $cm^{-2}$ $s^{-1}$, M1 = 10 x C1. Note the decline in activity, with only minor flares after the 12th.

Figure 9. Region History. The number of spots is indicated by the dark triangle in (a) and by the asterisks in (b). The solid lines represent sunspot area evolution. The flare histograms at the bottom of the plots indicate the number and magnitude of the x-ray flares; open histograms for class C, lined for class M. In its first disk transit (a), the region was very small and non-productive of flares. As AR2665 (b), early activity had declined by mid transit and the region exhibited a gradual decline in sunspots and sunspot area.

Figure 10. Physical parameters (Equations 2-12, 2-11 and 2-13) for AR2665, determined using Lorentz equations and vector mganetograms obtained as a function of time and observing wavelength. Solid lines connect 120 mÅ observations, while simple 60 and 90 mÅ observations are also shown. Error bars are one sigma values determined as the square root of the sum over pixels of Equations 4-1, 4-3, and 4-2 respectively.

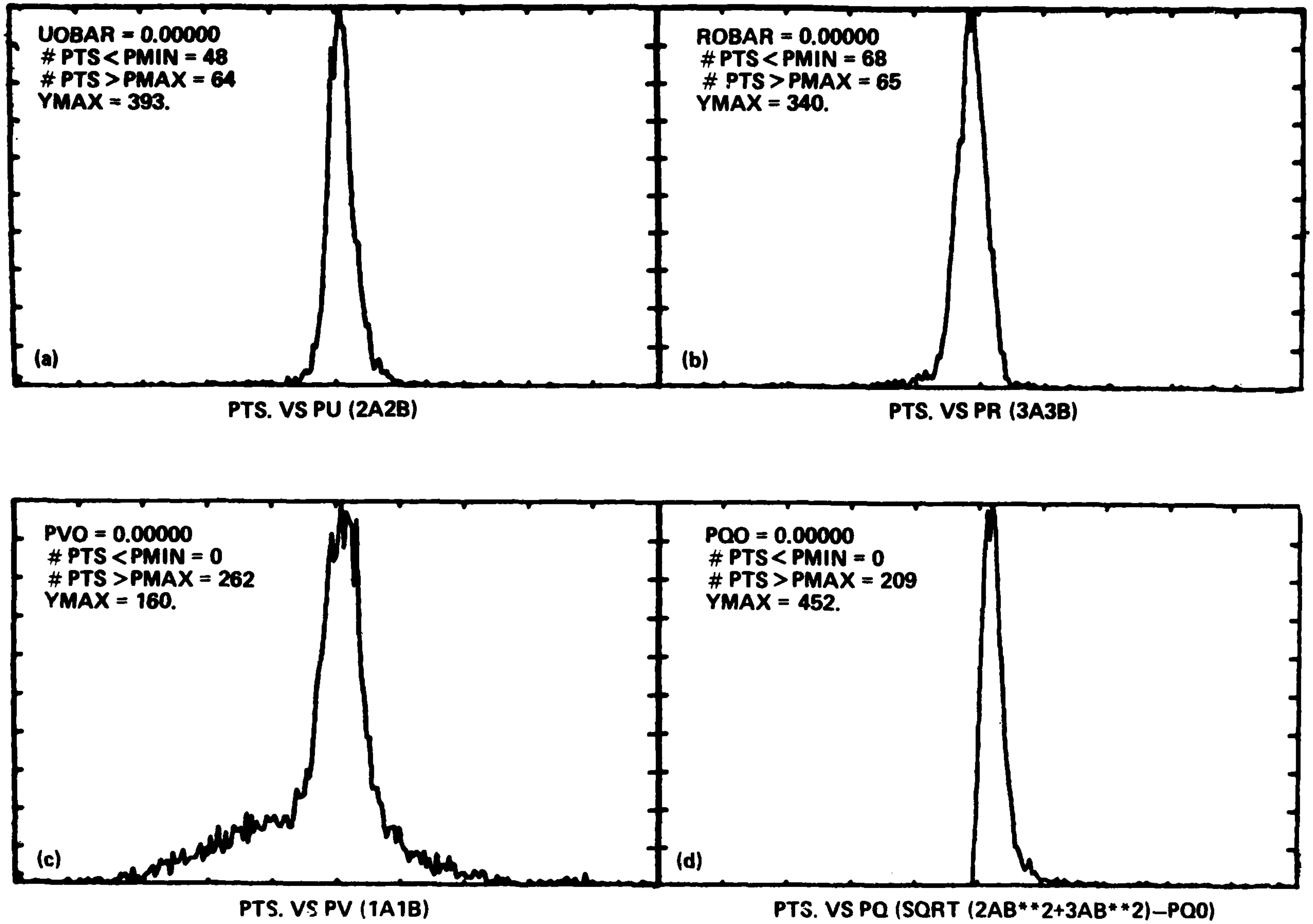
UOBAR = 0.00000
# PTS < PMIN = 48
# PTS > PMAX = 64
YMAX = 393.
(a)
PTS. VS PU (2A2B)
ROBAR = 0.00000
# PTS < PMIN = 68
# PTS > PMAX = 65
YMAX = 340.
(b)
PTS. VS PR (3A3B)
PVO = 0.00000
# PTS < PMIN = 0
# PTS > PMAX = 262
YMAX = 160.
(c)
PTS. VS PV (1A1B)
PQO = 0.00000
# PTS < PMIN = 0
# PTS > PMAX = 209
YMAX = 452.
(d)
PTS. VS PQ (SQRT (2AB**2+3AB**2)–PQ0)

Figure 1 a - d

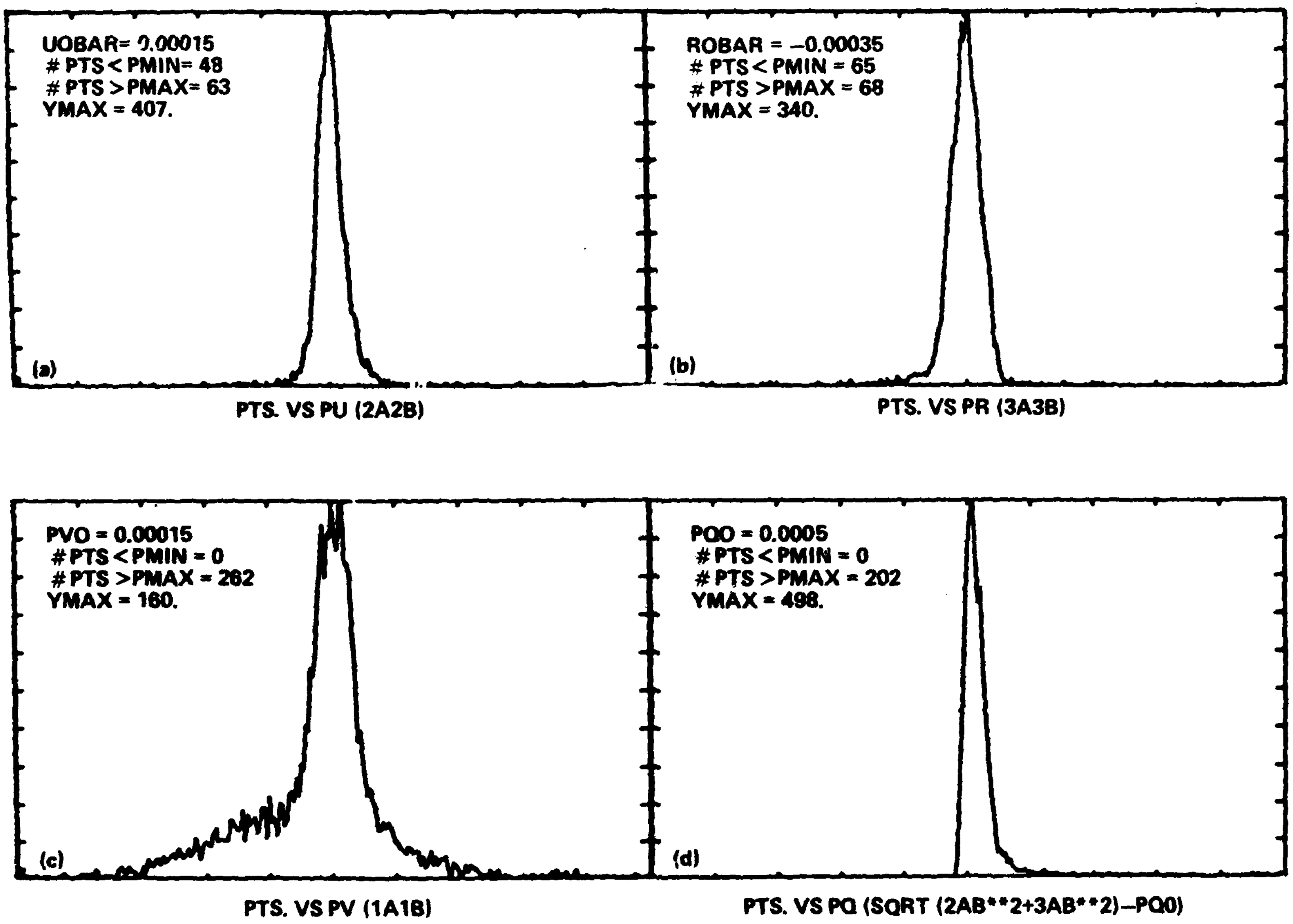
UOBAR= 0.00015
# PTS < PMIN= 48
# PTS > PMAX= 63
YMAX = 407.
(a)
PTS. VS PU (2A2B)
ROBAR = −0.00035
# PTS < PMIN = 65
# PTS > PMAX = 68
YMAX = 340.
(b)
PTS. VS PR (3A3B)
PVO = 0.00015
# PTS < PMIN = 0
# PTS > PMAX = 262
YMAX = 160.
(c)
PTS. VS PV (1A1B)
PQO = 0.0005
# PTS < PMIN = 0
# PTS > PMAX = 202
YMAX = 498.
(d)
PTS. VS PQ (SQRT (2AB**2+3AB**2)−PQ0)

Figure 2 a - d

15/1359 U.T. SEPT., 1980

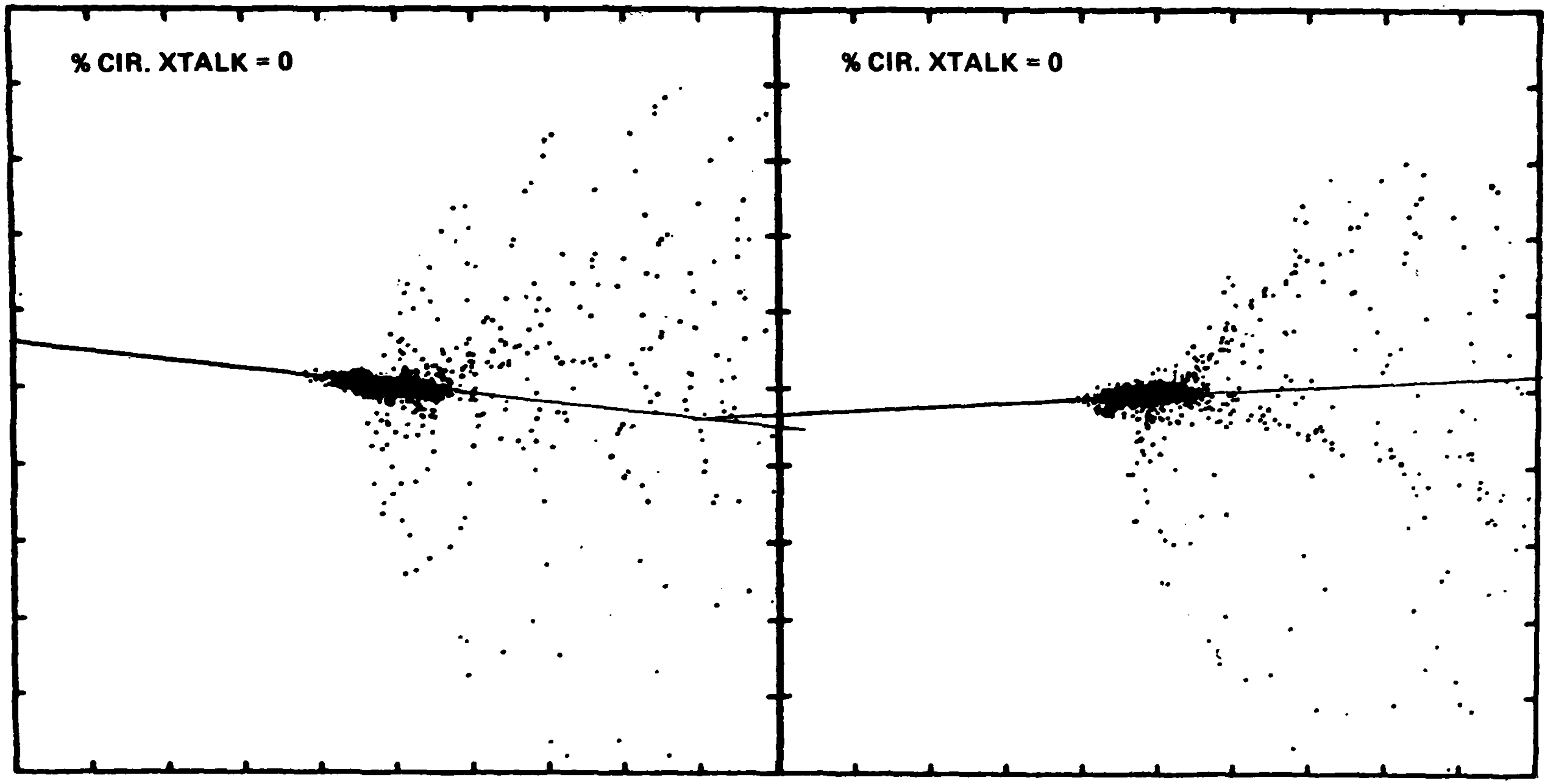


3A3B VS 1A1B

2A2B VS 1A1B

Figure 3 a - b

15/1359 U.T. SEPT. 1980

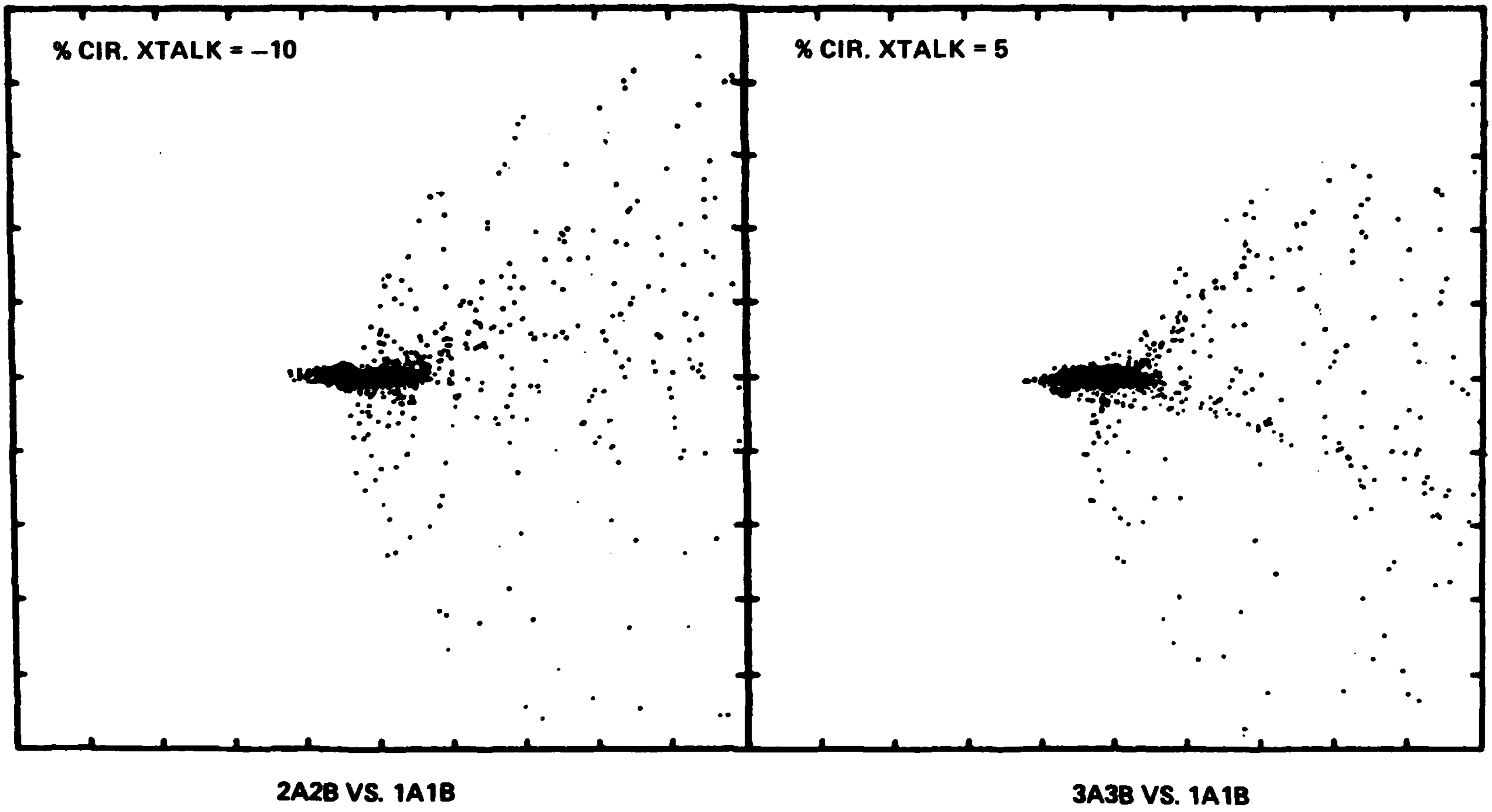


Figure 4 a - b

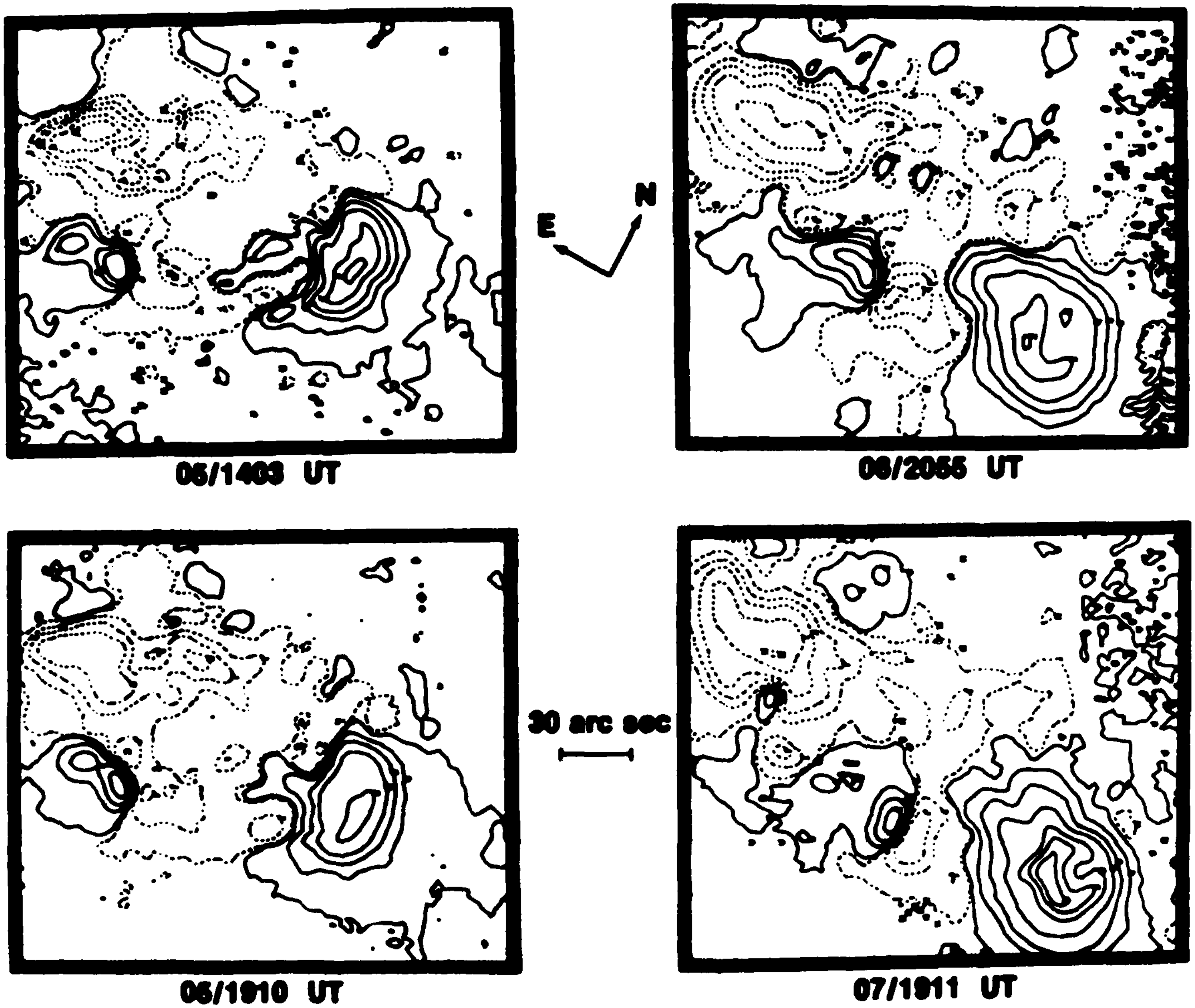


Figure 5

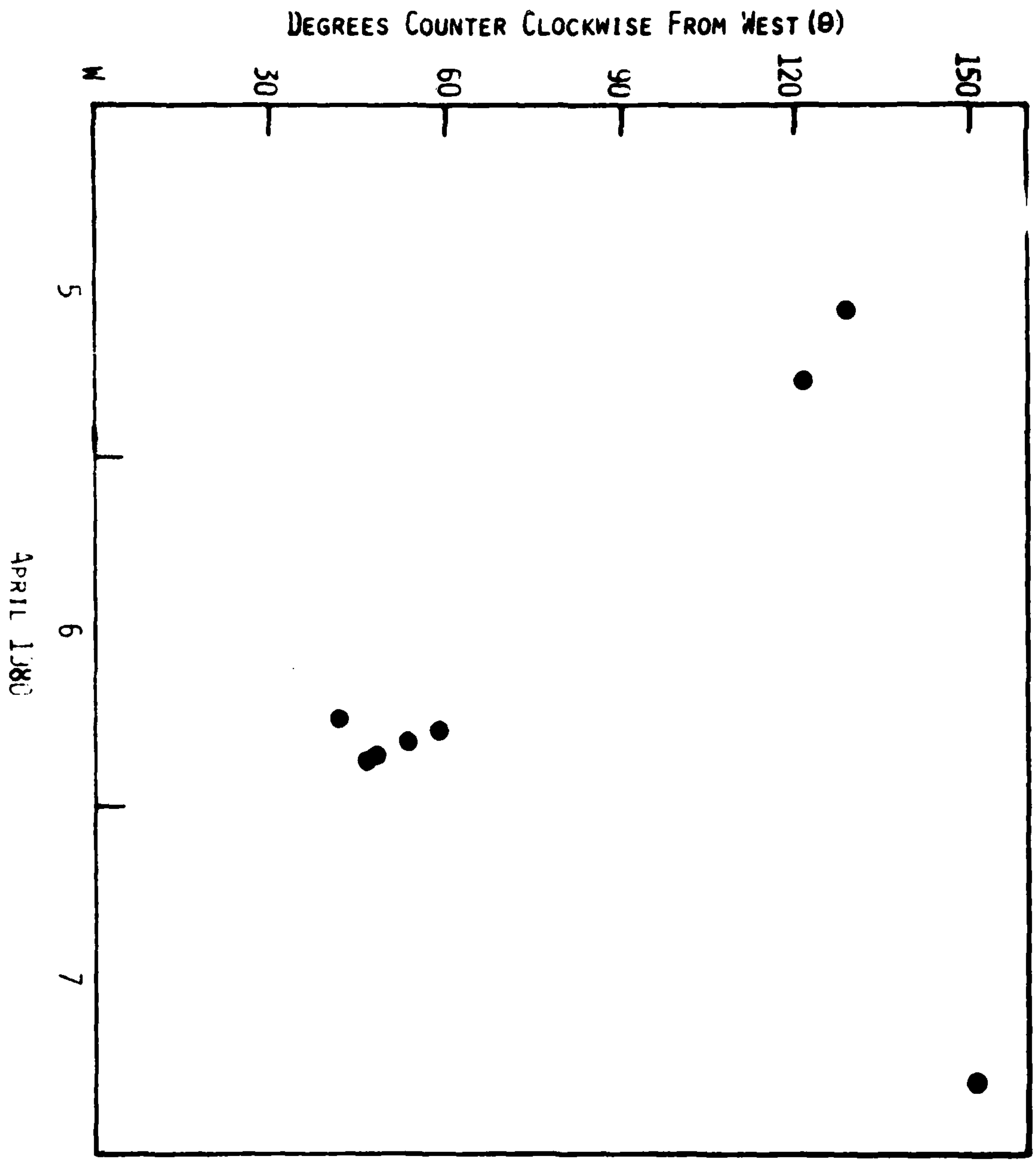
DEGREES COUNTER CLOCKWISE FROM WEST (θ)
W
30
60
90
120
150
5
6
7
APRIL 1980

Figure 6

15/1349 U.T. SEPT. 1980

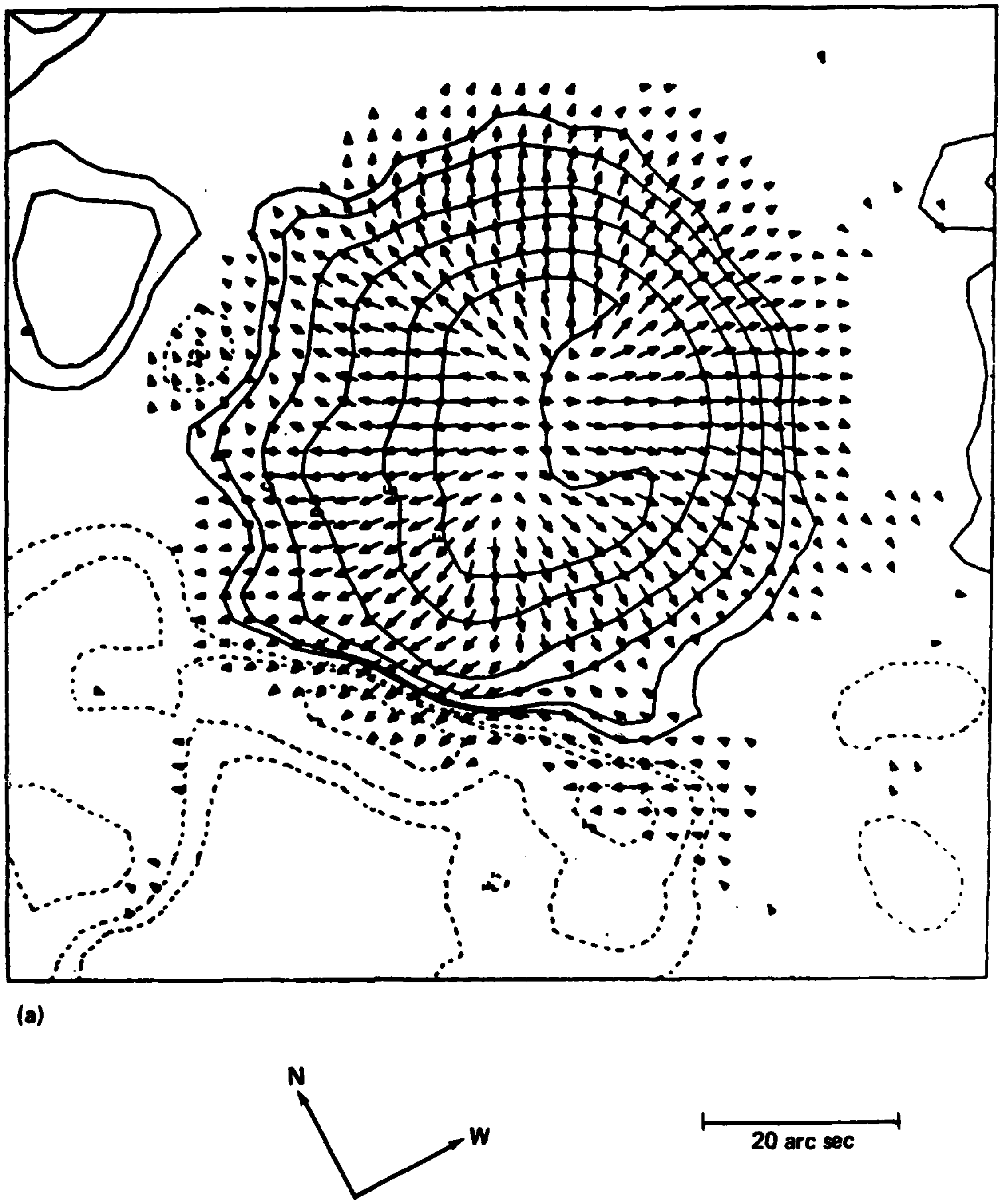


Figure 7 a

15/2029 U.T. SEPT. 1980

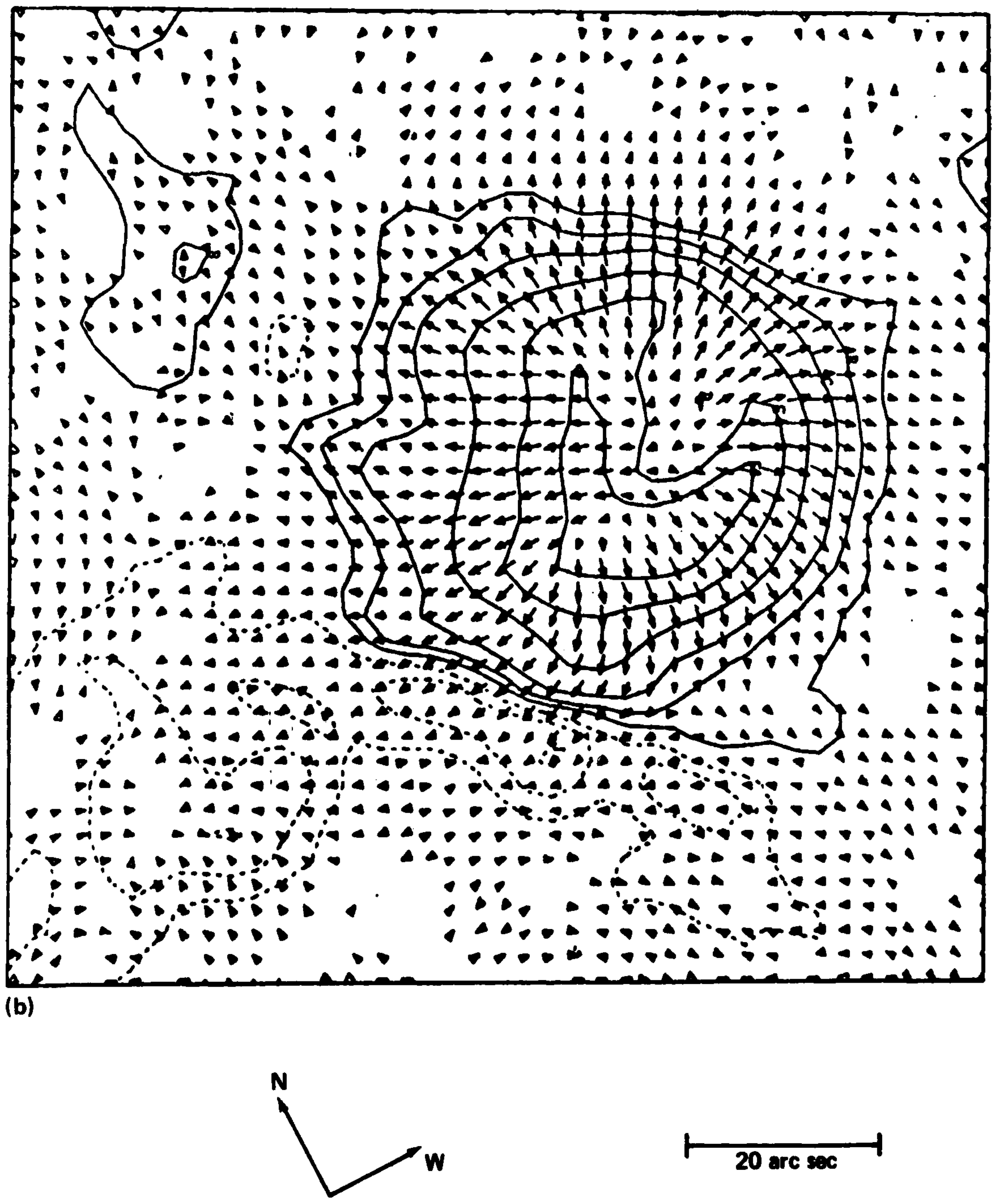


Figure 7 b

16/1359 U. T. SEPT. 1980

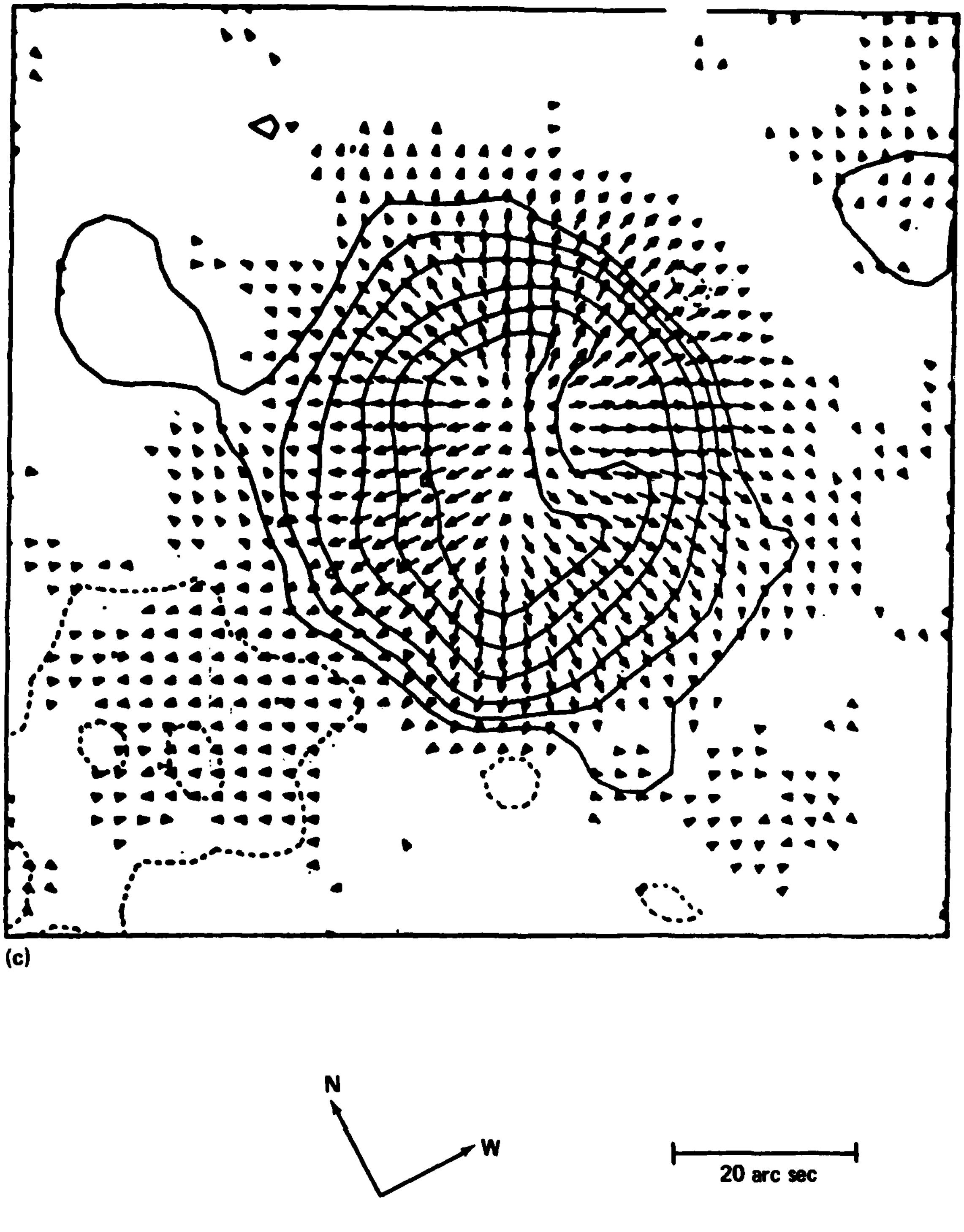


Figure 7 c

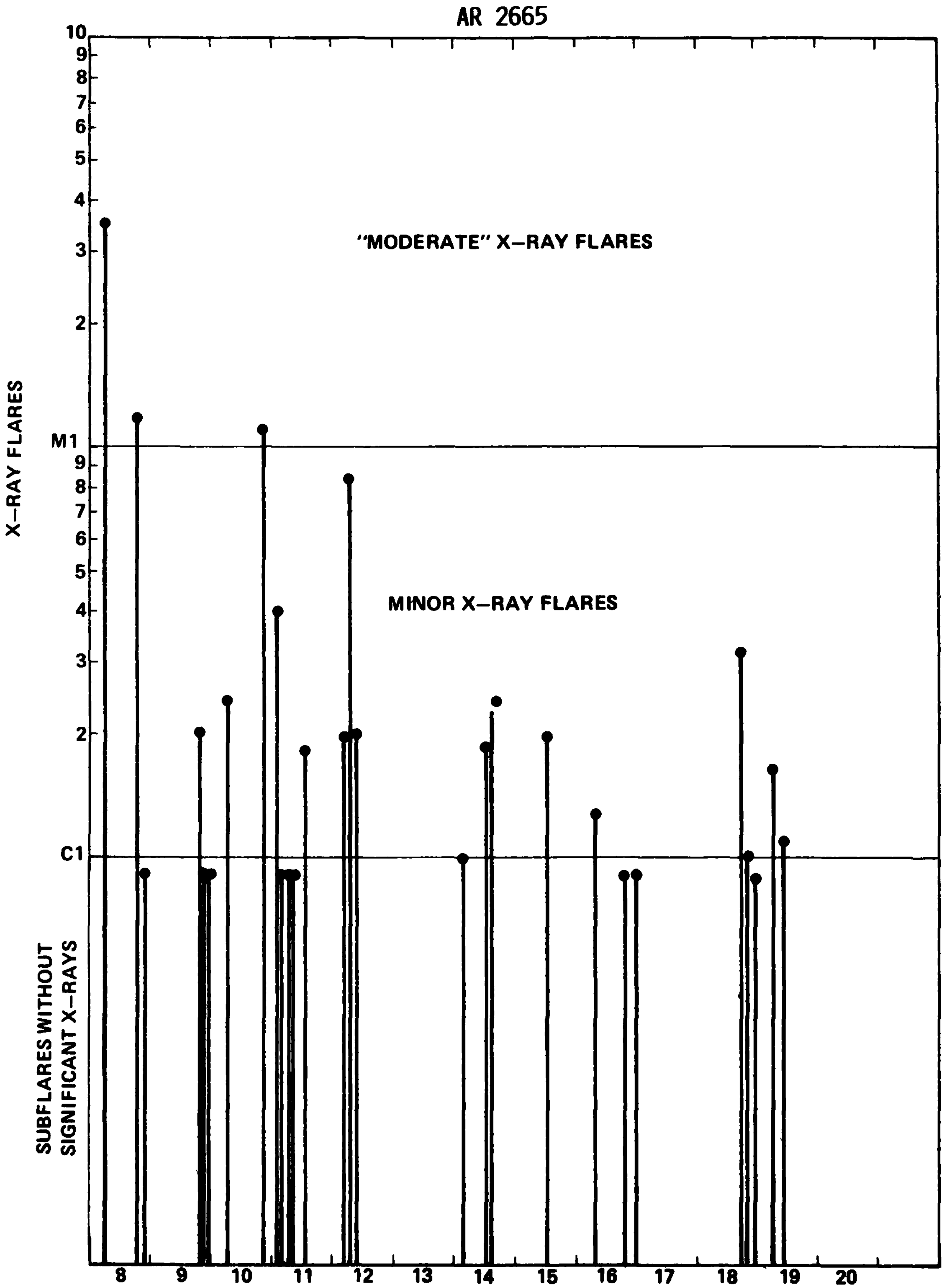

AR 2665
"MODERATE" X-RAY FLARES
MINOR X-RAY FLARES
X-RAY FLARES
SUBFLARES WITHOUT SIGNIFICANT X-RAYS
10
9
8
7
6
5
4
3
2
M1
9
8
7
6
5
4
3
2
C1
8
9
10
11
12
13
14
15
16
17
18
19
20


Figure 8

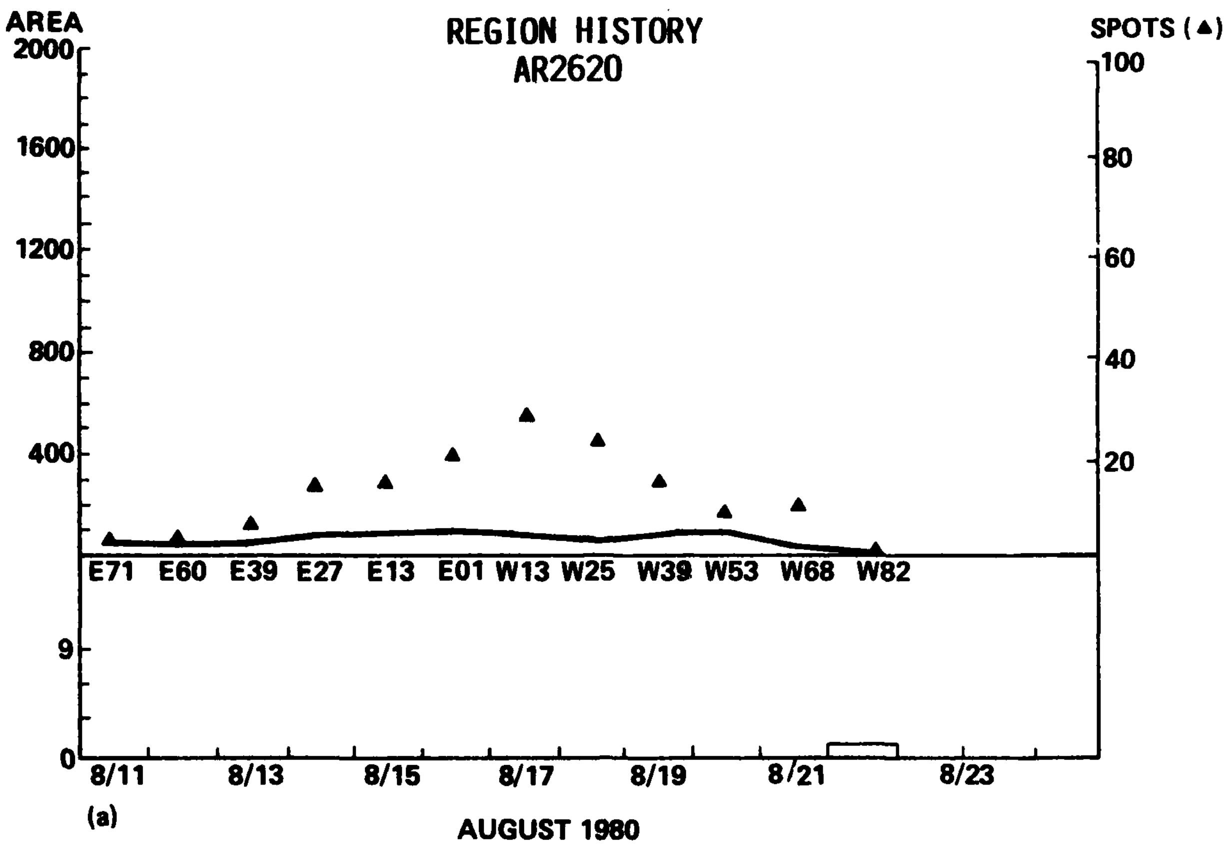
AREA
REGION HISTORY
AR2620
SPOTS (▲)
2000
1600
1200
800
400
100
80
60
40
20
E71 E60 E39 E27 E13 E01 W13 W25 W39 W53 W68 W82
9
0
8/11 8/13 8/15 8/17 8/19 8/21 8/23
(a)
AUGUST 1980

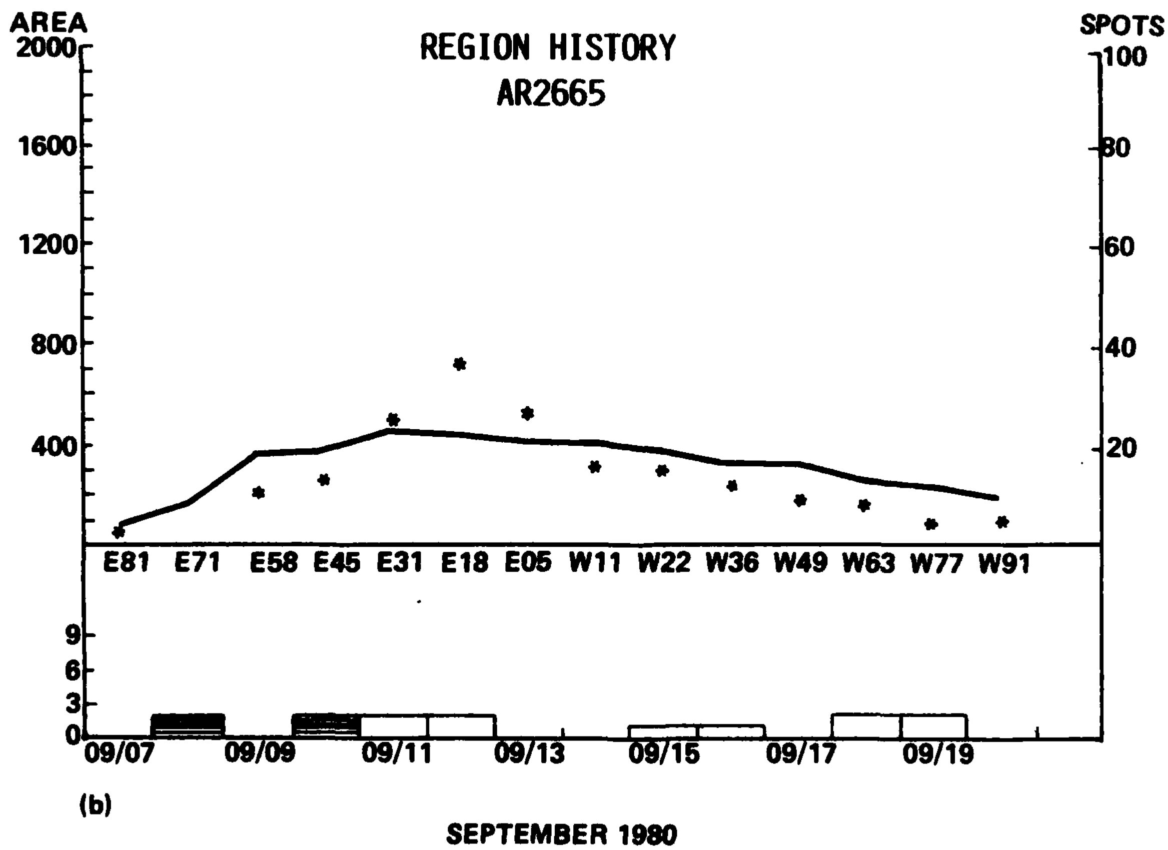
AREA
REGION HISTORY
AR2665
SPOTS
2000
1600
1200
800
400
100
80
60
40
20
E81 E71 E58 E45 E31 E18 E05 W11 W22 W36 W49 W63 W77 W91
9
6
3
0
09/07 09/09 09/11 09/13 09/15 09/17 09/19
(b)
SEPTEMBER 1980

Figure 9

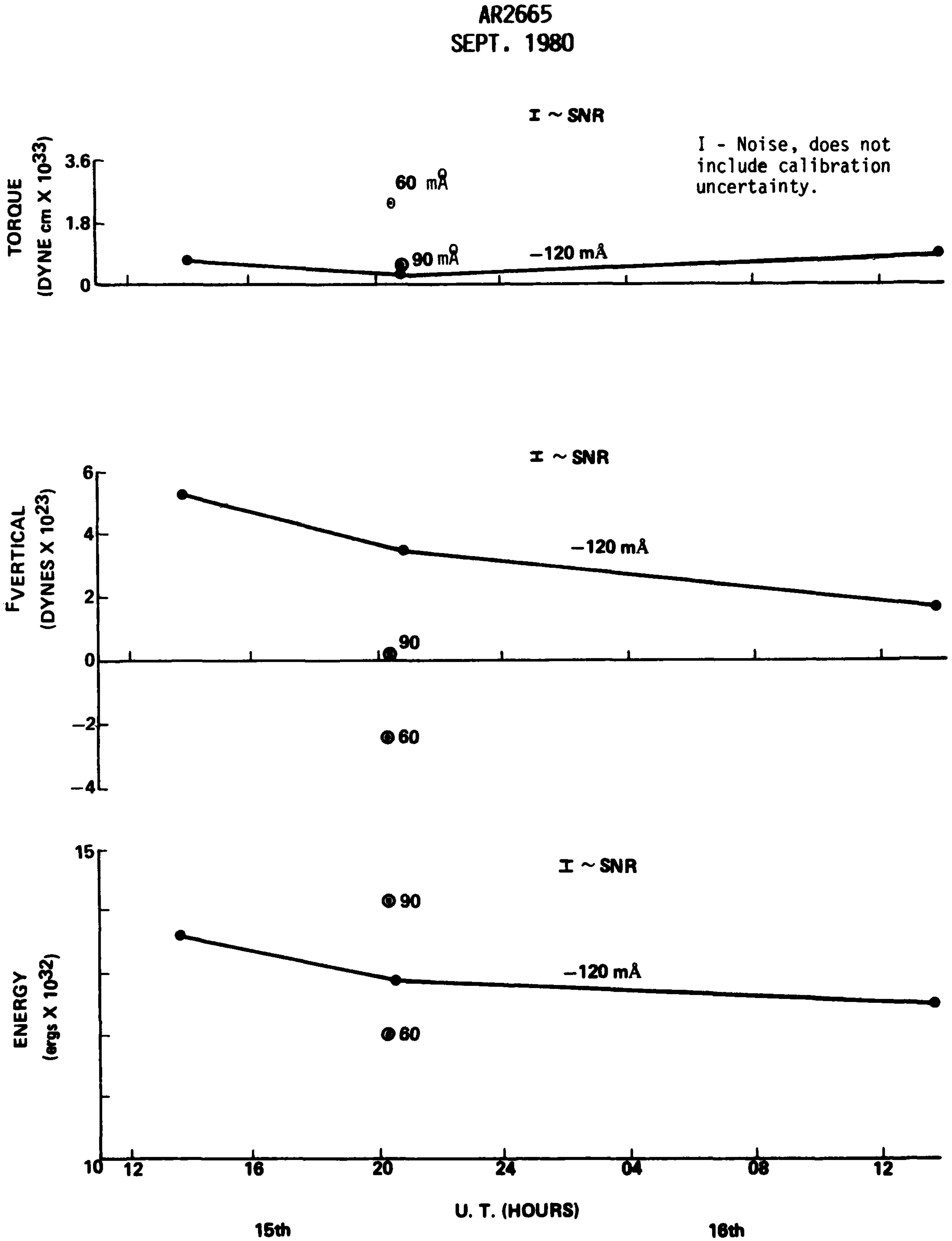
AR2665
SEPT. 1980
I ~ SNR
I - Noise, does not include calibration uncertainty.
TORQUE
(DYNE cm X 10^33)
3.6
1.8
0
60 mÅ
90 mÅ
-120 mÅ
I ~ SNR
F VERTICAL
(DYNES X 10^23)
6
4
2
0
-2
-4
-120 mÅ
90
60
I ~ SNR
ENERGY
(ergs X 10^32)
15
10
90
-120 mÅ
60
12
16
20
24
04
08
12
U. T. (HOURS)
15th
16th

Figure 10

TABLE I. MSFC Magnetograph Optical Configuration For Measuring Circular And Linear Polarizations

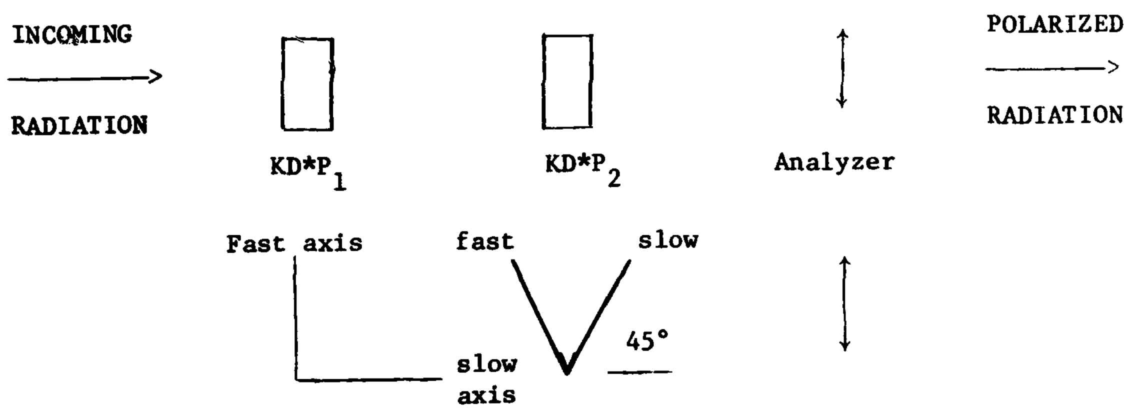


| Intensity | | | Polarization | |
|---|---|---|---|---|
| I1 | 0λ | +λ/4 | I + V | $P_V$ |
| I2 | 0λ | -λ/4 | I - V | |
| I3 | λ/4 | +λ/4 | I + U | U |
| I4 | λ/4 | -λ/4 | I - U | |
| I5 | 0λ | 0λ | I + Q | R |
| I6 | 0λ | λ/2 | I - Q | |

References

1. Tanaka K. and Nakagawa, Y. 1973, Solar Phys, 33, 187 "Force-free Magnetic Fields and Flares of August 1972".

2. Hagyard, M. J. 1976 (unpublished)

3. Levine, R. H. 1976, Solar Physics, 46, 159 "Evidence for Opposed Currents in Active Region Loops".

4. Krall, K. R., Reichmann E. J., Wilson, R. M. Henze, W. and Smith, J. B., Jr. 1978, Solar Physics, 56, 383 "Analysis of X-ray Observations of the 15 June 1973 Flare in Active Region NOAA 131".

5. Molodensky, M. M. 1974, Solar Physics, 39, 393 "Equilibrium and Stability of Force-Free Magnetic Field".

6. Kjeldseth, Moe, O. 1968, Solar Physics, 4, 267 "A Generalized Theory for Line Formation in a Homogeneous Magnetic Field".

7. Krall, K. R., Smith, J. B., Jr., Hagyard, M. J., West, E. A. and Cumings, N. P. 1982, Solar Physics, 79, 59 "Vector Magnetic Field Evolution, Energy Storage, and Associated Photospheric Velocity Shear Within a Flare-Productive Active Region".

8. West, E. A. and Hagyard, M. J. 1983, Solar Physics, 88, 51 "Introduction of Vector Magnetograph Data Including Magneto-optic Effects".